Photoprotons from C^{12} and F^{19}†

K. M. MURRAY AND W. L. BENDEL
Nucleonics Division, U. S. Naval Research Laboratory, Washington, D. C.
(Received 18 June 1963)

The energy distributions of charged particles from C^{12} and from F^{19}, irradiated with 23.5-MeV bremsstrahlung from the Naval Research Laboratory betatron, have been measured using a silicon-diode charged-particle detector. The spectrum from carbon is found to consist largely of protons and shows no pronounced resonances. The spectrum from fluorine shows considerable structure, much of which is due to protons. There is evidence that this spectrum contains heavier charged particles.

INTRODUCTION

IT has long been felt that the photonuclear "giant resonance" contained fine structure. The first indication that such structure does exist came from very carefully measured activation curves for the (γ,n) process.[1–3] Breaks found in these curves were attributed to the onset of new levels of excitation appearing as the peak energy of the bremsstrahlung was raised. More direct evidence of this fine structure showed up in the measurement of the energy of protons from (γ,p) reactions. In general, nuclear emulsions were used to measure the energy of these photoprotons.[4–7] With this method it is very laborious to observe a statistically significant number of events. As a result of these limited statistics, much of the fine structure reported for the (γ,p) reactions is in doubt. For these reasons, a counter experiment was undertaken using silicon-diode charged-particle detectors to measure the charged-particle spectra from carbon and from fluorine.

EXPERIMENTAL APPARATUS

Figure 1 is a schematic representation of the arrangement of the 24-MeV NRL betatron, beam monitor, collimator, general shielding, target chamber, and evacuated beam pipe used in this experiment. In order to isolate the target chamber from the background produced by the betatron and the collimation, it was necessary to drill a hole in the building wall (5 ft of concrete), and to orient the betatron so as to aim the primary beam through this hole. The area outside the building is fenced in and contains a massive beam catcher so as not to endanger personnel in the vicinity.

The collimation system consisted of an 8-in. long brass cylinder with a $\frac{3}{4}$-in. hole, followed by an 8-in. lead cylinder with a tapered hole approximately $\frac{3}{8}$ in. diam. The lead collimator served to define the x-ray beam. The brass cylinder was used to reduce the total number of neutrons produced in collimation. The lead collimator was 1.1 m from the internal target of the betatron, i.e., the bremsstrahlung source. An air ion chamber was interposed between the collimator and the betatron as a beam monitor, the output of which was integrated as a measure of the total dose on the target. This position was necessary to make the leakage current (about 10^{-9} A) small compared to the current due to the x rays.

Following the collimator is a 2-in. diam vacuum pipe approximately 7 ft long with a 1.5-mil Mylar entrance window. This pipe is connected directly to the target chamber. The beam passes through this pipe, through the target chamber, into an additional section of pipe containing pump-out arms, and then exits through a second Mylar window. Thus, the beam path, from about 7 ft before the target to about 2 ft after the target, was at a pressure of about 10^{-2} Torr. The target foils were mounted in the center of the scattering chamber such that the beam passed through them at nearly grazing incidence. The detector was mounted inside the target chamber 10 cm from the center.

X-Ray Beam

One of the difficulties encountered in pulsed accelerators is the pile-up of events in the detector due to the high intensity during the short time that the beam is on. If one can make this time long compared to the resolving time of the detection system, one reduces the probability that two events observed by this system

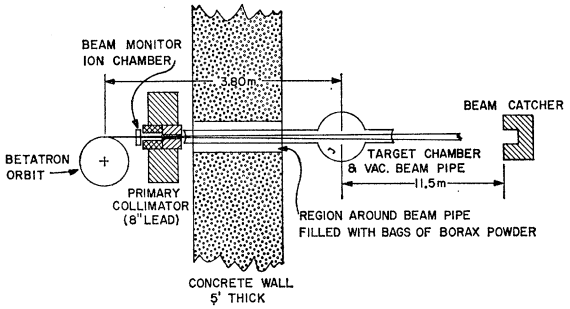

FIG. 1. The arrangement of the betatron, shielding, and target chamber.

† Submitted by K. M. Murray to the faculty of the Graduate School of the University of Maryland in partial fulfillment of the requirements for the degree of Master of Science, 1963.

[1] J. G. V. Taylor, L. B. Robinson and R. N. H. Haslam, Can. J. Phys. **32**, 238 (1954).
[2] L. Katz, R. N. H. Haslam, R. J. Horsley, A. G. W. Cameron, and R. Montalbetti, Phys. Rev. **95**, 464 (1954).
[3] J. Goldemberg and L. Katz, Phys. Rev. **95**, 471 (1954).
[4] L. Cohen, A. K. Mann, B. J. Patton, K. Reibel, W. E. Stephens, and E. J. Winhold, Phys. Rev. **104**, 108 (1956).
[5] D. L. Livesey, Can. J. Phys. **35**, 987 (1957).
[6] C. Milone, R. Ricamo and A. Rubbino, Nuovo Cimento **5**, 528 (1957).
[7] B. Forkman and I. Wahlström, Arkiv Fysik **12**, 339 (1960).

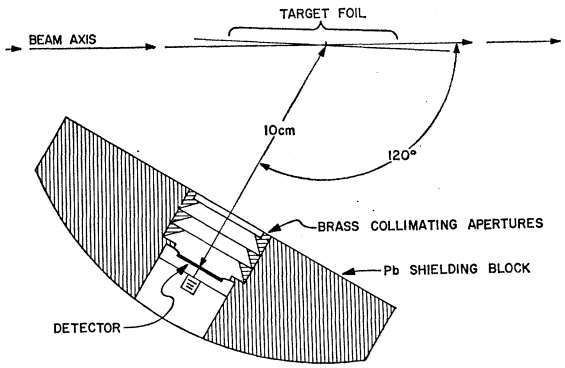

FIG. 2. The relative position of the target and the detector.

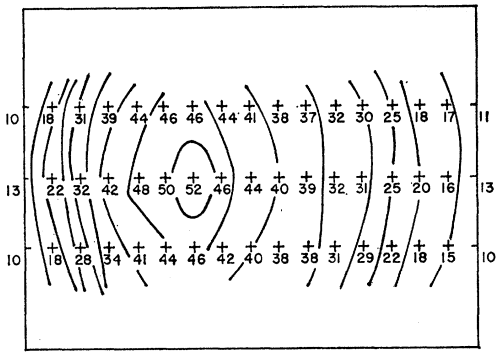

FIG. 3. The relative solid angle of the detector as viewed from points on the target. The numbers are in arbitrary units.

during a single x-ray burst will overlap in time. The normal operation of the NRL betatron is at 180 cycles/sec with a fast expansion of the electron beam orbit producing an x-ray burst of approximately 0.5-μsec duration. The time constant of the detector is about 0.1 μsec, but the decay constants for most charge-sensitive preamps are several μsec. Therefore, all particles produced by a short x-ray burst would be superimposed. Consequently, a system for producing an x-ray burst 150 to 300-μsec long was developed.[8] This long x-ray burst started about 200 μsec after the trigger from the energy selector of the betatron. Although the energy at which the energy selector triggered was constant, the peak energy of x rays produced some 200 or 300 μsec later would depend upon the amplitude of the betatron magnetic field.

The beam intensity was measured by means of a 25-R thimble ion chamber inserted in a block of Lucite such that there was at least 6 cm of Lucite in all directions around the R thimble.[9] The R thimble, in its Lucite block, was placed in several positions to measure the beam intensity. All of these measurements agreed to within 5% when corrected by the inverse square of the distance. The current integrator of the beam monitor was thereby calibrated for the x-ray dose incident upon the target foil in the scattering chamber.

Target Chamber

The target chamber is a simple cylindrical vacuum chamber, made of aluminum, 15 in. i.d. and 6 in. deep. The target foils were mounted in the center of the chamber by horizontal bars placed above and below the beam and sufficiently widely spaced to clear the beam. Thus, no material other than the target foil itself was allowed in the beam. The entrance window to the target chamber was a 1.5-mil Mylar foil located approximately 7 ft from the target chamber, as shown in Fig. 1. The exit window was about 2 ft from the center of the target chamber. Neither window was visible to the detector.

[8] K. M. Murray, M. S. thesis, University of Maryland, 1963 (unpublished).
[9] Nat. Bur. Std. U. S. Handbook **55** (1954).

The target foil for carbon was approximately 1 mil of polyethylene in a sheet 4 in. long and 3 in. high. The area was measured and the total foil was weighed in order to determine its average thickness, 2.50 ± 0.02 mg cm^{-2}. For fluorine, a polytetrafluoroethylene (CF_2) foil of similar dimensions by 0.5 mil thick was used. The weight and area measurements gave a value of 3.00 ± 0.03 mg cm^{-2}. The CF_2 foil did not appear to be as uniform as the polyethylene foil. However, these nonuniformities could not be detected with an ordinary micrometer. The target foils were placed in the target chamber as shown in Fig. 2, making an angle of about 3° with the axis of the beam. Thus, the central region of the target foil was irradiated over its entire length.

Detector

The detector was mounted in a lead brick with brass collimating apertures placed as shown in Fig. 2. This internal shielding was found very helpful in reducing the background. The distance from the center of the target chamber to the face of the detector was 10 cm, and the detector was at an effective angle of 118° with respect to the beam axis. The detector was a surface-barrier solid-state charged-particle detector of 3 cm^2 area made from 6000 Ω-cm material, and could be operated with a

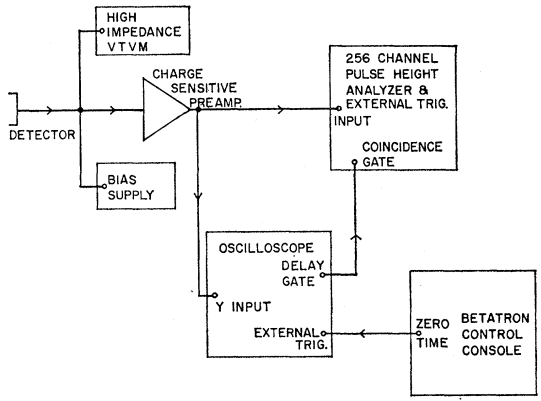

FIG. 4. Block diagram of the electronics employed in the collection of data.

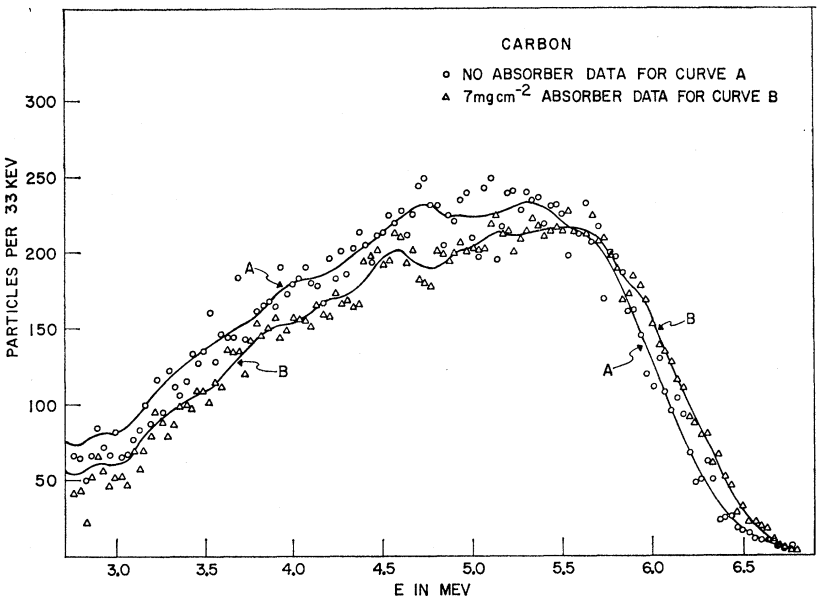

FIG. 5. Pulse-height distributions from carbon. Curve A is the smoothed value of the data taken with no absorber between target and detector. Curve B is the smoothed value of the data taken with 7 mg cm^{-2} of aluminum between target and detector. The absorber data has been corrected at each point for the energy lost in the absorber by a proton of that energy.

maximum bias voltage of 200 V. This resulted in a maximum depletion depth of 550 μ, which is the range of an 8.8-MeV proton. Since particles could enter the detector at angles approaching 35° from the normal, protons with energies as high as 10.5 MeV were stopped by this depletion depth. This is particularly evident in the CF_2 data. The resolution of the detector at maximum operating voltage was 85-keV full width at half-maximum for a 5.8-MeV alpha particle.

As is apparent from Fig. 2, the detector was capable of seeing all of the target but not with a uniform solid angle. Therefore, a device was constructed such that the alpha source could be moved about in the plane of the target and its apparent intensity measured, thus allowing a topography of the detector's ability to "see" the target to be mapped. This is shown in Fig. 3. Each point was measured to an accuracy of about 10%. The integral of this topography over the irradiated area, normalized to the solid angle computed for the center of the target, represents the effective solid angle times area of the target.

Electronic Circuitry

The detector was connected to a low-noise charge-sensitive preamplifier. Since the leakage current in the detector was found to vary from about 0.75 μA to a little more than 1.0 μA with variations in ambient temperature and humidity, a high-impedance voltmeter was placed directly across the detector to monitor the bias voltage. This leakage current caused a large voltage drop across the 23-MΩ supply resistor in the preamplifier and, without the monitoring voltmeter, would have made the actual bias voltage uncertain. This would result in an unknown thickness of the depletion region in the detector. The output of the preamplifier was connected to the low-level input of a 256-channel pulse-height analyzer.

Figure 4 is the block diagram of the electronics used in this experiment. The input to the pulse-height analyzer was displayed on an oscilloscope. This instrument provided a 300-μsec gate signal from its delayed-sweep system, gating the analyzer on only during the x-ray pulse.

MEASUREMENTS AND RESULTS

Carbon

For the measurements of the carbon yield, a polyethylene foil 2.50±0.02 mg cm^{-2} thick was used as a target. It was apparent in early runs with the carbon data that the spectrum cut off rather sharply at about 7 MeV. It was, therefore, decided to lower the bias voltage on the detector to 78 V in order to decrease the thickness of the sensitive region of the detector, and thereby reduce its sensitivity to electrons. The background without the target in the chamber was extremely low. With the target present it was found that the pulses below about 2.5 MeV were due predominantly to electrons from the target. The yield in this region was many times the yield without a target in the chamber. When background runs were made, with 10 mils of aluminum foil interposed between the detector and the target, the yield in the region up to 2.5 MeV was almost unchanged while the yield beyond this point was reduced essentially to zero. This was thick enough to stop the most energetic protons anticipated from this target.[10] The decrease in bias voltage gave about a 30% reduction in background. The resolution of the experimental setup was estimated to be about 200 keV for 5.5 MeV protons.

[10] M. Rich and R. Madey, Range-Energy Tables, UCRL 2301, 1954 (unpublished).

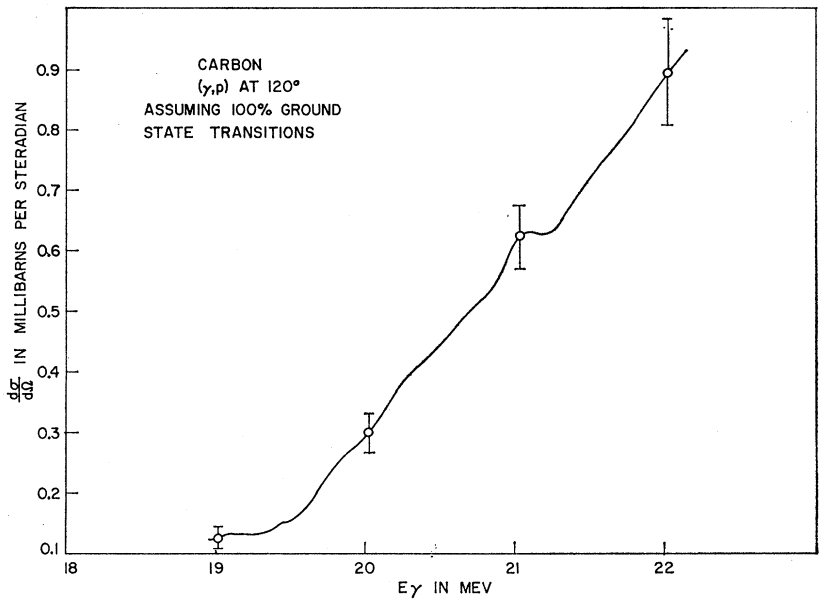

FIG. 6. The differential cross section for the $C^{12}(\gamma,p)B^{11}$ reaction from 19 MeV to 22 MeV assuming 100% ground-state transitions.

This spread was mostly due to the thickness of the target. A gain setting of 33 keV/channel was chosen to spread the carbon data over approximately 200 channels. At this gain setting a total of 66 "runs" were required to produce approximately 230 counts in the peak channels. A "run" consisted of 5000 counts on the ion chamber integrator and required approximately 1h. In the initial set of runs on carbon, background runs were made alternately with data runs. It became apparent that this procedure was a considerable waste of time since there was so little background above 2.5 MeV. After this, background runs were taken only once in about 5 or 6 runs.

Curve A of Fig. 5 is the pulse-height distribution for the 66 runs on carbon. The energy scale is based on the calibration of the detector by the alpha source, and the linearity and zero channel determined by pulser measurements. The data were smoothed by averaging with a weighting function of 155-keV full width at half-maximum. The smooth curve is provided to make it somewhat easier to see the trend of the data, the weighting function being based upon the resolution of the experiment.

The data appear to drop off sharply after a broad maximum in the interval between 5 and 6 MeV. This is because the maximum proton energy at this angle is limited to about 6.8 MeV by the 23.5 MeV bremsstrahlung. Previous measurements[5,6,11,12] of the carbon spectrum with higher energy accelerators show a proton yield maximum in the vicinity of 6 MeV.

This spectrum represents not simply protons from carbon but all charged particles ejected from the target (electron background having been removed). Since the threshold for alpha emission is only 7.3 MeV, a great part of the bremsstrahlung is available for producing this particle. Therefore, the carbon measurements were repeated using an aluminum absorbing foil 7 mg cm^{-2} thick interposed between the target and detector. This foil could be swung into position such that the detector would look at the target through the foil. When calibration was desired, the Po^{210} alpha source was swung into position.

A total of 103 runs were made with the 7 mg cm^{-2} absorber, resulting in approximately 350 counts in the peak channels. The 7 mg cm^{-2} absorber will just stop a 6.2-MeV alpha particle. The results of these runs are plotted on Fig. 5 as curve B. These data have been normalized to the same x-ray dose on the target foil as the 66 no-absorber runs, and have been corrected in energy at each point as if they were due to protons. One can see that curve B is slightly lower than curve A up to about 5.5 MeV and then is higher in the steeply descending region. Curves A and B are nearly parallel in the descending region, indicating that the average bremsstrahlung peak energy for curve B was about 0.1 MeV greater than for curve A. This was due to a slightly better adjustment of the betatron as the experiment progressed. Such a change will cause only a very small error in the calculated cross section provided one does not use the values near the high-energy limit.

Since the maximum photon energy was about 23.5 MeV, only (γ,p) and (γ,α) reactions would be observed from carbon. (The photoproton contribution from the deuterium in the target is negligible.) Therefore curve B of Fig. 5 is due almost entirely to protons, while the low-energy portion of curve A contains alpha particles. If we assume that all the protons observed, curve B, represent transitions from excited states of the C^{12}

[11] W. R. Dodge and W. C. Barber, Phys. Rev. **127**, 1746 (1962).
[12] E. Finckh, R. Kosiek, K. H. Lindenberger, K. Maier, U. Meyer-Berkhout, M. Schechter, and J. Zimmerer, preliminary results from Physics Institute, Heidelberg (unpublished).

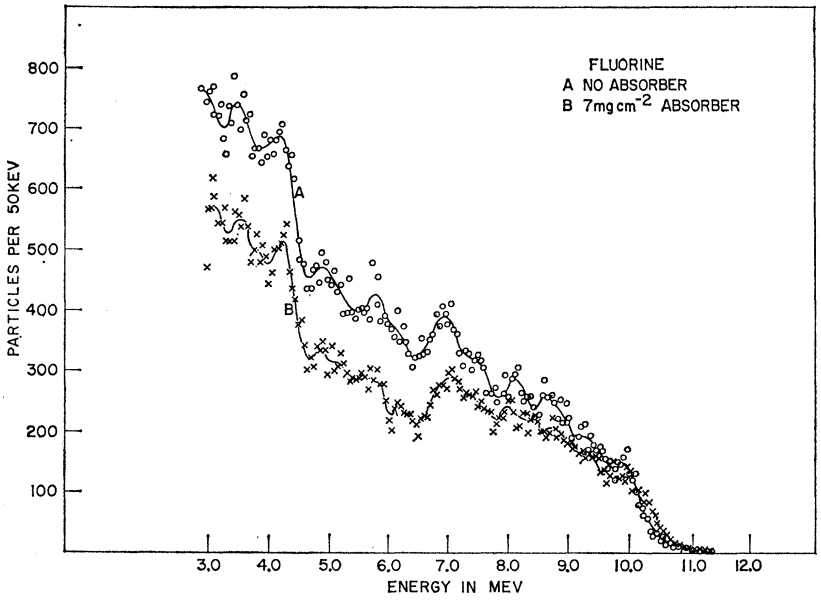

FIG. 7. Pulse-height distributions from fluorine. Curve A represents the smoothed value of data taken with no absorber. Curve B represents the smoothed value of data taken with 7 mg cm^{-2} of aluminum between target and detector, and was corrected in the same manner as in Fig. 5.

nucleus to the ground state of the B^{11} nucleus, we can then calculate the differential cross section, $d\sigma/d\Omega$, for this reaction. Figure 6 shows the results of this calculation. The values are in good agreement with those observed by Dodge and Barber[11] over the energy range where these data and their data overlap.

Fluorine

In order to observe charged particles from photons interacting with the fluorine nucleus, a foil of polytetrafluoroethylene (CF_2), 3.00±0.03 mg cm^{-2} thick, was substituted for the polyethylene foil. As the yield from carbon had already been measured, it was subtracted from the yield from CF_2 and the remainder was assumed to be due to fluorine. Curve A of Fig. 7 is the fluorine pulse height spectrum taken in 108.5 runs. The gain employed in collecting the fluorine data was 50 keV/channel to accommodate proton energies as high as 10 MeV. The data were smoothed as previously described for carbon.

Here again, this picture represents all charged particles from the fluorine nucleus. The thresholds[13] for the various particle reactions in F^{19} are given in Table I. As can be seen from this Table, many particles can be produced by 23.5-MeV bremsstrahlung.

TABLE I. Thresholds of F^{19} reactions.

Reaction	Threshold[a] (MeV)
$F^{19}(\gamma,\alpha)N^{15}$	4.012
$F^{19}(\gamma,p)O^{18}$	7.992
$F^{19}(\gamma,n)F^{18}$	10.442
$F^{19}(\gamma,t)O^{16}$	11.699
$F^{19}(\gamma,d)O^{17}$	13.814

[a] See Ref. 13.

[13] *Nuclear Data Sheets*, compiled by K. Way *et al.* (Printing and Publishing Office, National Academy of Sciences–National Research Council, Washington 25, D. C.).

In order to gain some information concerning the nature of the particles which produced the fluorine spectrum, the 7 mg cm^{-2} Al absorber was used, again for 108.5 runs. In order to cancel the effects of any systematic changes, as observed in the carbon data, the absorber and no-absorber runs were alternated. These data, again corrected for background due both to electrons and carbon, are also shown in Fig. 7 as curve B. Curve B was corrected at each point for the energy loss of a proton passing through the aluminum.

Since the total dose incident upon the target for curves A and B of Fig. 7 was the same, it is apparent that a large fraction of those particles counted in curve A were not observed in the second spectrum, curve B. The gross features of curve A are reflected in curve B, but there is a noticeable change in the energy interval from 5 to 7 MeV. This is a strong indication that the data observed in this interval are not due exclusively to protons. In order to make these differences more apparent, the sum and difference data are plotted for fluorine in Fig. 8. The difference data appear to show some structural features which are statistically significant. Since any structure due to alpha particles would be spread over several MeV due to the thickness of the target, they could not produce the structure observed. It seems reasonable to assume that this structure indicates the presence of deuterons and/or tritons. These difference data show a negative region in the vicinity of 10.5 MeV, which is due to protons which passed through the detector in the no-absorber case while stopping in the detector for the absorber measurements. None of the prominent peaks of curve A can be identified with the shift expected for either deuterons

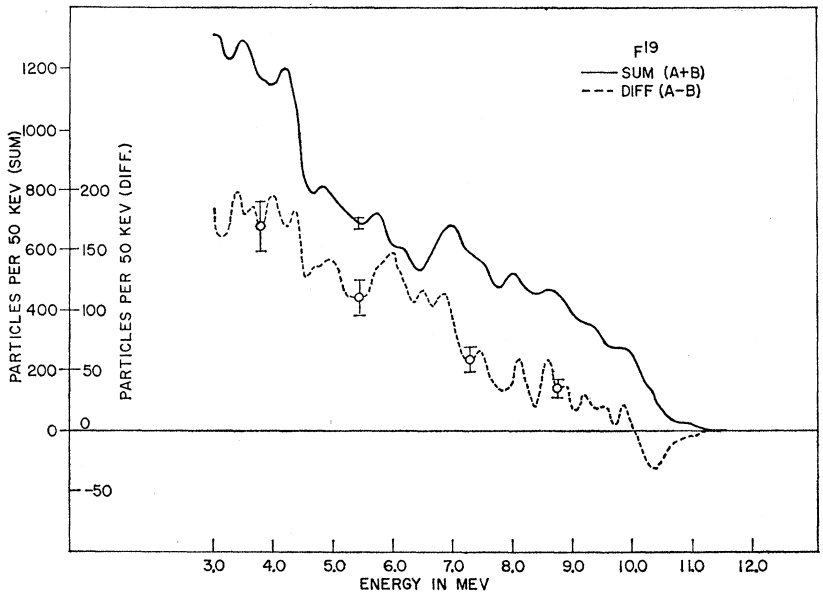

FIG. 8. The continuous curve represents the sum of curves A and B of Fig. 7, plotted against the outer scale at the left. The dashed curve is the difference (A−B), plotted against the inner scale.

or tritons, but do in fact agree with the shift calculated for protons. These peaks, however, contain a considerable non-proton component.

CONCLUSIONS

Carbon

Several workers[4–6,11,12,14] have studied the carbon (γ,p) spectrum. Cohen *et al.*[4] report possible levels in the C^{12} nucleus at energies of 17.3, 20.8, and 21.5 MeV due to proton groups observed at 1.3, 4.8, and 5.3 MeV. Livesey[5] observed possible peaks at proton energies of 5.3 and 6.0 MeV, while the Heidelberg group[12] observed the possibility of peaks at 3.1, 4.9, and 5.9 MeV. Dodge and Barber,[11] using the electron beam from the Stanford Mark II linear accelerator to study (e,pe') reactions, observed no significant structure for proton energies below 6 MeV. Their work is of approximately the same resolution as the present work, and represents statistical sampling at least as great.

Figure 6 does not show any structure which stands out above statistical error. There is, however, a small hump at 21.05 MeV. This corresponds to a proton energy of 4.7 MeV. It is interesting to note that Dodge and Barber also observe an equally insignificant hump at exactly the same energy. Whether this is mere coincidence, or a real resonance, can only be determined by further experimental measurements of better resolution and statistics.

Fluorine

The yield from fluorine was $(3.5\pm0.3)\times10^5$ charged particles, with energies greater than 3 MeV, per gram-atom per R of 23.5-MeV bremsstrahlung. It has already been pointed out that the fluorine data contains particles other than protons. For this reason, no differential cross section as a function of energy has been calculated from these data. Such a calculation would have no meaning and could not be compared with any similar calculation by other observers.

Figure 9 is an energy level diagram[13] of the F^{19} nucleus showing the thresholds for several of the reactions which could be produced by 23.5-MeV bremsstrahlung. Also shown in this figure is the energy distribution of photons in 23.5-MeV bremsstrahlung, plotted on the same energy scale. The many levels in the F^{19} nucleus below the (γ,p) threshold have been left out of the diagram since they are not pertinent to this discussion. The region from the (γ,p) threshold to the 11.80-MeV state contains many levels spaced much too closely to be

TABLE II. Proton energies and F^{19} levels, in MeV.

			F^{19*} to O^{18} ground state		
E_p	F^{19*} to O^{18}	F^{19*} to O^{18*}	Dodge[a] (e,pe')	Fork-man[b] (γ,n)	Other (γ,n)
(2.98)			11.42	11.4	11.5[c,d]
3.58±0.06	11.80	15.44 to 3.63			
			11.90	11.9	11.9[c,d]
4.28±0.06	12.55				12.2[c]
			12.74	12.8	
(4.97)					
				13.6	
5.83±0.06	14.19				
(6.23)		(16.60 to 1.98)			
6.97±0.05	15.41			15.4	15.3[c,d]
			15.70		
(7.53)					
8.10±0.08	16.61			16.5	
(8.65)					

[a] See Ref. 11. [c] See Ref. 1.
[b] See Ref. 7. [d] See Ref. 3.

[14] J. Halpern and A. K. Mann, Phys. Rev. **83**, 370 (1951).

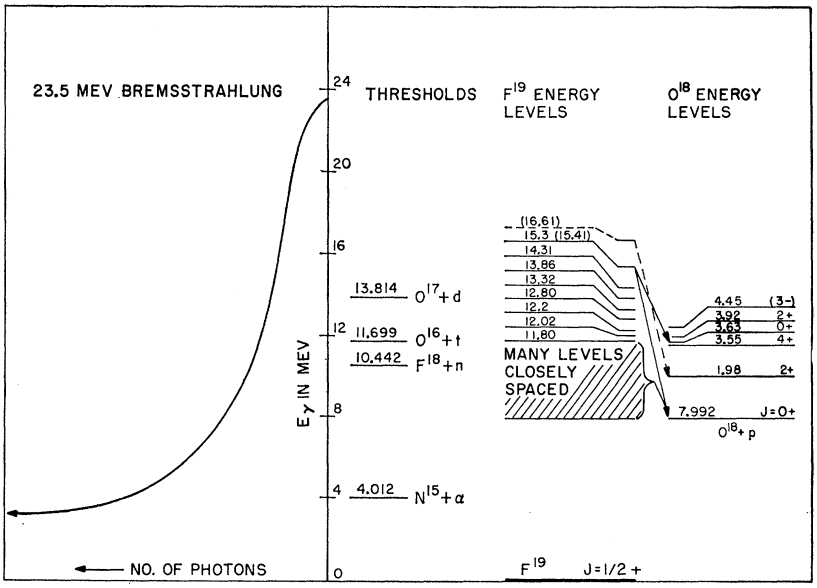

FIG. 9. The energy distribution of the bremsstrahlung beam is plotted on the same energy scale as the F^{19} thresholds and the energy levels of the F^{19} and O^{18} nuclei. Levels of F^{19} below the proton threshold have been omitted for the sake of clarity.

resolved by this experiment. This contributes to the very high yield in the region below 4 MeV. Also shown on this figure are arrows from certain levels in F^{19} to levels of O^{18}, showing possible transitions observed by the authors.

The first column of Table II is a list of the energies of proton groups observed here, after correcting for the thickness of the CF_2 foil. The values shown in parentheses are for peaks which do not stand out strongly and are therefore questionable. The second column lists the excited levels of the F^{19} nucleus assuming that the residual nucleus is left in its ground state.

The most prominent proton group is at 6.97 MeV. This energy corresponds to a transition from a level of F^{19} at 15.41 MeV to the ground state of O^{18}. The Saskatchewan group[1,3] shows a level at 15.3 MeV from (γ,n) data. The proton group at 3.58 MeV fits a transition from a level in F^{19} at 15.44 MeV to an excited state of O^{18} at 3.63 MeV[13] (see column 3 of Table II). Both the ground state of O^{18} and the level at 3.63 MeV are 0^+ states which is consistent with both these levels being fed from the same state in F^{19}. The 3.58 MeV proton group also corresponds to a transition to the ground state of O^{18} from a state in F^{19} at 11.80 MeV, in agreement with the known 11.80-MeV level.[13] The 3.58-MeV protons may be due partly or entirely to such a transition.

The proton group at 8.10 MeV corresponds to a ground state transition from a level in F^{19} at 16.61 MeV. The small group at 6.23 MeV could also be attributed to such a level decaying to the 2^+ state at 1.98 MeV in O^{18}. The 16.61-MeV level is shown in Fig. 9 as a dashed line since no level above 15.3 MeV is listed.[13]

The proton peaks at 4.28 MeV and at 5.83 MeV do not correspond to transitions from known F^{19} levels. These peaks may be unresolved proton groups due to transitions from known levels in F^{19} to known levels in O^{18}.

ACKNOWLEDGMENTS

The authors would like to thank Dr. Harry Holmgren and Dr. John McElhinney for their helpful suggestions concerning the experimental apparatus.